

First neutron Bragg-edge imaging experimental results at CSNS

Jie Chen(陈洁), Zhijian Tan(谭志坚), Weiqiang Liu(刘玮强), Sihao Deng(邓司浩), Shengxiang Wang(王声翔), Liyi Wang(王立毅), Haibiao Zheng(郑海彪), Huaile Lu(卢怀乐), Feiran Shen(沈斐然), Jiazheng Hao(郝嘉政), Xiaojuan Zhou(周晓娟), Jianrong Zhou(周健荣), Zhijia Sun(孙志嘉), Lunhua He(何伦华), and Tianjiao Liang(梁天骄)
Citation: Chin. Phys. B, 2021, 30 (**9**): 096106. DOI: 10.1088/1674-1056/ac0da7
Journal homepage: http://cpb.iphy.ac.cn; http://iopscience.iop.org/cpb

What follows is a list of articles you may be interested in

Effects of deuteration on the structure of $NH_4H_2PO_4$ crystals characterized by neutron diffraction

Baoan Liu(刘宝安), Lili Zhu(朱丽丽), Fafu Liu(刘发付), Xun Sun(孙洵), Xiping Chen(陈喜平), Lei Xie(谢雷), Yuanhua Xia(夏元华), Guangai Sun(孙光爱), Xin Ju(巨新)
Chin. Phys. B, 2019, 28 (**1**): 016103. DOI: 10.1088/1674-1056/28/1/016103

The interplay between the lattice and magnetism in $La(Fe_{11.4}Al_{1.6})C_{0.02}$ studied by powder neutron diffraction

Wang Zhi-Cui,He Lun-Hua,Wang Hai,Liu Rong-Deng,Wang Fang-Wei
Chin. Phys. B, 2012, 21 (**4**): 046101. DOI: 10.1088/1674-1056/21/4/046101

Neutron diffraction study on composite compound Nd_2Co_7

Yang Yu-Qi, Li Guan-Nan, Wang Tong, Huang Qing-Zhen, Gao Qing-Qing, Li Jing-Bo, Liu Guang-Yao, Luo Jun, Rao Guang-Hui
Chin. Phys. B, 2011, 20 (**10**): 106101. DOI: 10.1088/1674-1056/20/10/106101

RAPID COMMUNICATION

First neutron Bragg-edge imaging experimental results at CSNS*

Jie Chen(陈洁)[1,2,4,†], Zhijian Tan(谭志坚)[1,2], Weiqiang Liu(刘玮强)[1,2,4], Sihao Deng(邓司浩)[1,2], Shengxiang Wang(王声翔)[1,2], Liyi Wang(王立毅)[1,2], Haibiao Zheng(郑海彪)[1,2], Huaile Lu(卢怀乐)[1,2], Feiran Shen(沈斐然)[2,3,4], Jiazheng Hao(郝嘉政)[1,2], Xiaojuan Zhou(周晓娟)[1,2], Jianrong Zhou(周健荣)[1,2], Zhijia Sun(孙志嘉)[1,2], Lunhua He(何伦华)[2,3,‡], and Tianjiao Liang(梁天骄)[1,2]

[1] *Institute of High Energy Physics, Chinese Academy of Sciences (CAS), Beijing* 100049, *China*
[2] *Spallation Neutron Source Science Center (SNSSC), Dongguan* 523803, *China*
[3] *Beijing National Laboratory for Condensed Matter Physics, Institute of Physics, Chinese Academy of Sciences, Beijing* 100190, *China*
[4] *University of Chinese Academy of Sciences, Beijing* 100049, *China*

(Received 23 April 2021; revised manuscript received 13 June 2021; accepted manuscript online 23 June 2021)

The neutron Bragg-edge imaging is expected to be a new non-destructive energy-resolved neutron imaging technique for quantitatively two-dimensional or three-dimensional visualizing crystallographic information in a bulk material, which could be benefited from pulsed neutron source. Here we build a Bragg-edge imaging system on the General Purpose Powder Diffractometer at the China Spallation Neutron Source. The residual strain mapping of a bent Q235 ferrite steel sample has been achieved with a spectral resolution of 0.15% by the time-of-flight neutron Bragg-edge imaging on this system. The results show its great potential applications in materials science and engineering.

Keywords: neutron Bragg-edge imaging, China Spallation Neutron Source

PACS: 61.05.Tv, 61.05.F– **DOI:** 10.1088/1674-1056/ac0da7

Neutron diffraction usually provides average crystallographic and magnetic structure of crystalline materials over large volumes (usually cm^3 range) exposed to the neutron beam.[1–3] Bragg edges in the transmission spectrum are caused by diffracted neutrons from polycrystalline materials. d_{hkl} is the interplanar spacing (d-spacing) of the crystal lattice plane (hkl) and λ is the incident neutron wavelength. According to the Bragg's law $2d_{hkl}\sin(\theta) = \lambda$, there are no diffracted neutrons beyond the wavelength $\lambda = 2d_{hkl}\sin(\pi/2)$, where 2θ is the scattering angle. The so-called Bragg edge appears as a sharp edge at $\lambda = 2d_{hkl}$ in the transmission spectrum. The neutron Bragg-edge imaging provides the possibility to spatially exploit the coherent scattering structural information of a sample in real space with high spatial resolution down to 50 μm. Two-dimensional (2D) or three-dimensional (3D) distributions of crystallographic phase, texture, strain, dislocation, and crystallite size could be extracted to study materials especially for engineering, batteries, metals, and alloys.[4–11] With the development of methodologies, detectors, and neutron sources, Bragg-edge imaging experiments have been achieved at both continuous reactor source and accelerator-driven pulsed neutron source, which has been developed to be a unique tool for materials scientists. Using a two-dimensional position-sensitive detector based on the time-of-flight (TOF) method[12] at a pulsed neutron source is considered to be the most efficient way for Bragg-edge imaging. Therefore, neutron imaging instruments with Bragg-edge imaging mode have been expected to be built at world-leading pulsed spallation neutron sources. Now, the pulsed neutron imaging instrument RADEN at J-PARC in Japan[13] and IMAT at ISIS[14] in UK have already started the user program. Energy-resolved neutron imaging instrument (ERNI) at China Spallation Neutron Source (CSNS)[15] in China, ODIN at ESS in EU,[16] and VENUS at SNS in USA are still under construction.

In this paper, a TOF Bragg-edge imaging system built on the General Purpose Powder Diffractometer (GPPD) at CSNS is introduced. The performance of Bragg-edge imaging at CSNS is evaluated by using several steel samples. The 2D strain mappings of a bent sample are given by calculating the changes of the Bragg-edge positions. The spectral resolution of transmission spectra is studied by comparing with neutron diffraction experiment. This work could contribute to the development of neutron imaging technologies and their applications, as well as demonstrate the feasibility of the Bragg-edge imaging on ERNI at CSNS.

The physical design[17] and the first experimental results[18] of GPPD were previously described. The decou-

*Project supported by the National Key Research and Development Program of China (Grant Nos. 2017YFB0701903 and 2016YFA0401502), the National Natural Science Foundation of China (Grant No. 12041202), the Youth Innovation Promotion Association of Chinese Academy of Sciences (Grant No. 2017023), the Guangdong Natural Science Foundation, China (Grant No. 2016A030313129), and the Department of Science and Technology of Guangdong Province under grant project of energy-resolved neutron imaging instrument.

†Corresponding author. E-mail: chenjie@ihep.ac.cn
‡Corresponding author. E-mail: lhhe@iphy.ac.cn

© 2021 Chinese Physical Society and IOP Publishing Ltd

pled poisoned hydrogen moderator is selected for GPPD. The diffraction sample position in a vacuum chamber is 30 m from the moderator to achieve high spectral resolution. For Bragg-edge imaging experiments, a pinhole selector and a imaging sample stage are installed at 28.4 m and 33.4 m from the moderator, respectively. There are vacuum flight tubes and a diffraction sample chamber between the pinhole selector and imaging sample stage as shown in the engineering design of the Bragg-edge imaging system in Fig. 1. The finally used pinhole selector with diameters $D = 5$, 10, and 20 mm yields collimation ratios of $L/D = 1000$, 500, 250 for a given flight path from the pinhole to the sample of $L = 5$ m. The sample stage has a rotation range of $\pm 135°$, XY motion range of ± 50 mm, and Z motion range of ± 10 mm. Two types of neutron detectors could be installed downstream of the sample stage. A CCD based neutron detector combined with scintillation screen is used to perform conventional neutron imaging.[19] A TOF neutron detector using ceramic gas electron multiplier (GEM) with 1.56 mm pixel size is used to perform Bragg-edge imaging experiments in this research.[20]

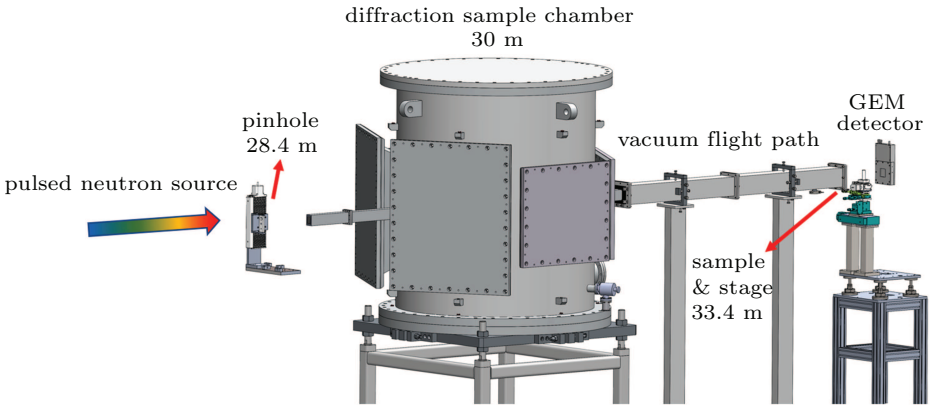


Fig. 1. Engineering design of the TOF Bragg-edge imaging system on GPPD.

To experimentally demonstrate the Bragg-edge imaging on this system, we choose Q235 ferrite steel (body-centered cubic structure, bcc) and 304 stainless steel (face-centered cubic structure, fcc) plate and bent samples to perform Bragg-edge imaging experiments. The samples are placed at 3 cm in front of the GEM neutron detector as shown in Fig. 2(a). The optical image of steel samples are shown in Fig. 2(a) with a distance of 3 cm between samples and detector. The thicknesses of the plate and bent samples are 9 mm and 28.4 mm, respectively. Based on the TOF method, the Bragg-edge transmission (BET) data of each GEM detector pixel is collected in event mode. The measurement time is 14.4 hours at a proton beam power of 25 kW at CSNS. Figure 2(b) gives the conventional neutron imaging by integrating the intensity of each pixel, which shows the attenuation contrast of the samples.

The BET event data of each pixel is finally converted to BET spectra through a routine reduction procedure. The BET spectra of Q235 ferrite steel plate with a thickness of 9 mm and 304 stainless steel plate with a thickness of 12 mm are plotted in Figs. 3(a) and 3(b), respectively. Theoretical BET curves have also been calculated by using pure α-Fe and γ-Fe,[21] as shown in Figs. 3(c) and 3(d) for comparing indexing. According to the Beer–Lambert law, the BET pattern is calculated by the formula $\mathrm{Tr}(\lambda) = I/I_0 = \mathrm{e}^{-N\sigma(\lambda)t}$, where I_0 is the incident beam, I is the transmitted beam, N is the number of scattering centers per unit volume, $\sigma(\lambda)$ is the total neutron cross section, and t is the thickness of the sample. Obviously, the measured transmission spectra can be indexed well by the bcc and fcc structures, respectively.

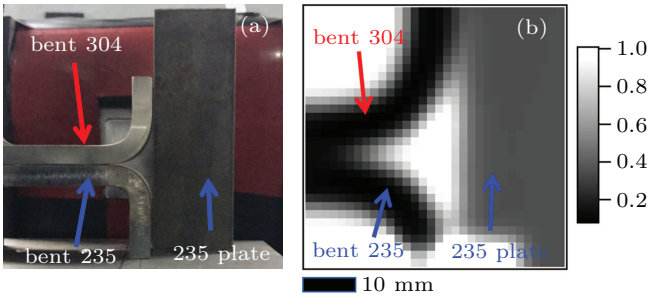


Fig. 2. (a) Optical image and (b) conventional neutron image of the steel samples.

In order to confirm the quality of the BET spectra, the diffraction experiment of Q235 ferrite steel has also been performed at GPPD. Diffraction pattern is obtained by the backscattering bank with scattering angle 2θ from 130° to 171°. Each Bragg edge of the BET spectra is matched well with the Bragg peak of the diffraction pattern, as exhibited in Figs. 4(a) and 4(c). The spectral resolution of the Bragg-edge imaging mode is evaluated by fitting the differential of (110) edge using the pseudo-Voigt function which could achieve 0.15% as shown in Fig. 4(b). The spectral resolution of the diffraction mode is calculated to be 0.17% by fitting the (110) peak in Fig. 4(d). The spectral resolution of Bragg-edge imaging mode and diffraction mode is consistent with each other.

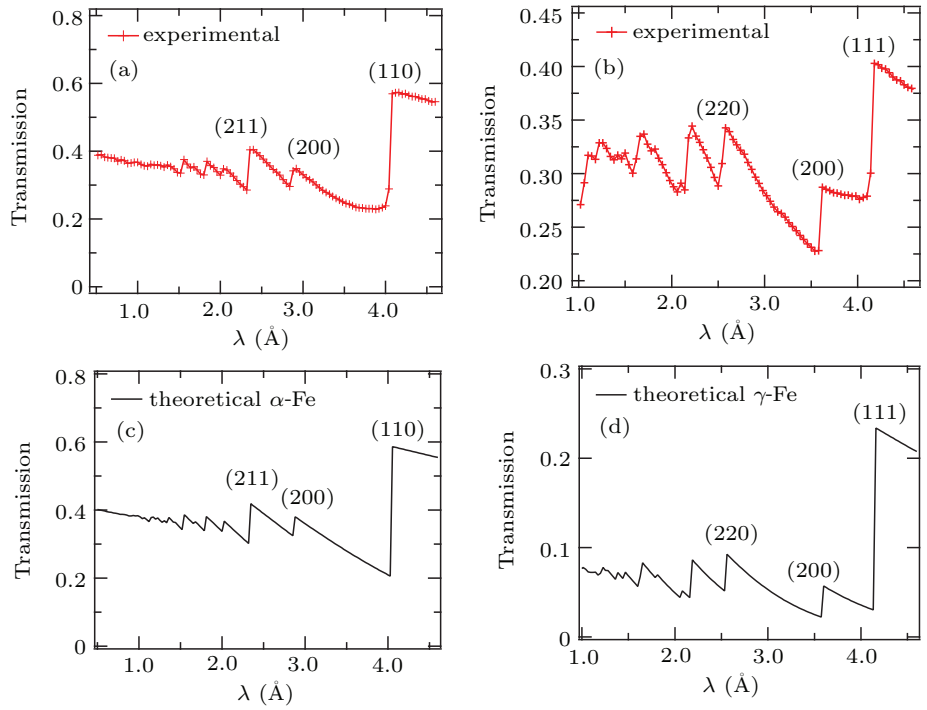


Fig. 3. (a) and (b) Experimental BET spectra of the Q235 and 304 steels. (c) and (d) Theoretical BET spectra of the α-Fe and γ-Fe.

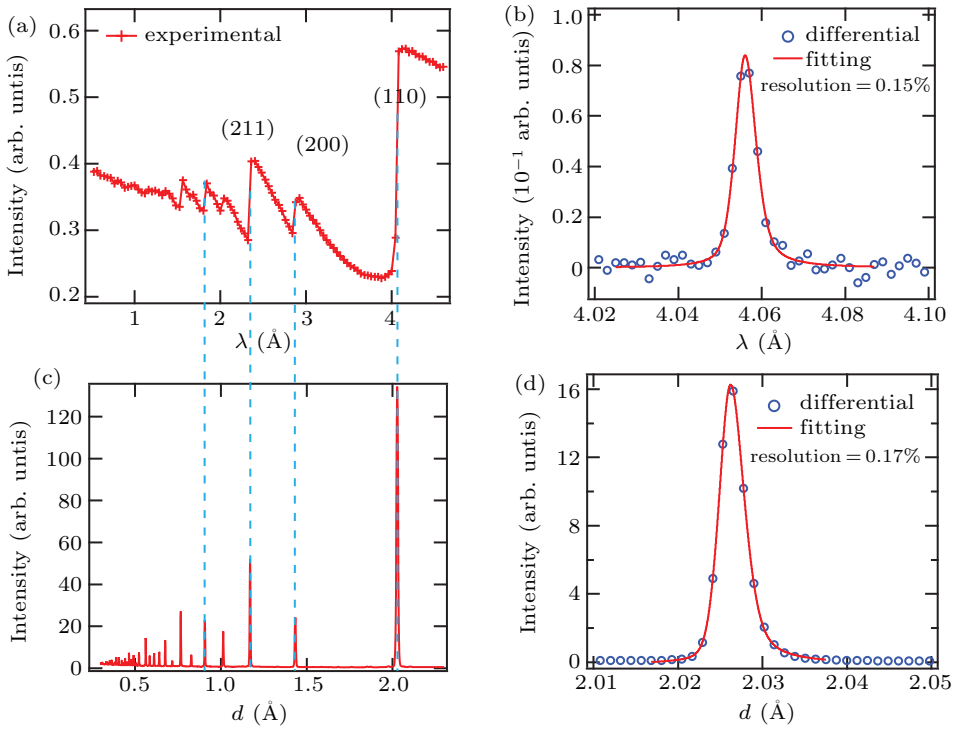


Fig. 4. (a) and (c) Experimental BET spectra and diffraction pattern of the Q235 ferrite steel, respectively. (b) and (d) The spectral resolution of Bragg-edge imaging mode and diffraction mode, respectively.

The elastic strain ε in crystal lattice can be calculated based on the following equation:

$$\varepsilon = (d_{hkl} - d_{0,hkl})/d_{0,hkl}, \tag{1}$$

where $d_{0,hkl}$ is d-spacing without strain/stress. In Bragg-edge transmission imaging, the edges appear at $\lambda = 2d_{hkl}$, deducing from Bragg's law. A region of interest (ROI) in Fig. 5(a) of the bent Q235 ferrite steel sample is chosen to calculate the 2D spatial distribution of the residual strain. The BET spectra in ROI have been re-binned twofold (2×2 pixels) to ensure enough statistics. The strain mapping along the projection has been achieved by fitting the edges[6] and calculating their relative shifts pixel by pixel. Four points have been selected to illustrate the fitting results in Fig. 5(b). According to the previous works,[22–24] the distribution of strain/stress during loading in the bending experiment is tension at the outer zone and compression at the inner zone of the samples. While, after loading is removed, the macroscopic resid-

ual strain/stress distributes in a trend of tension–compression–tension–compression from the inner to the outer of the bent sample. The strain/stress distribution is caused by the elastic recovery and the non-uniform plastic deformation.[23] A strain–position curve in Fig. 5(d) has been plot based on our residual strain map (Fig. 5(c)), which is consistent with the trend reported in the previously mentioned works. Because of the relatively larger pixel size in the present work, we will improve the resolution and accuracy of the Bragg-edge imaging in the future work.

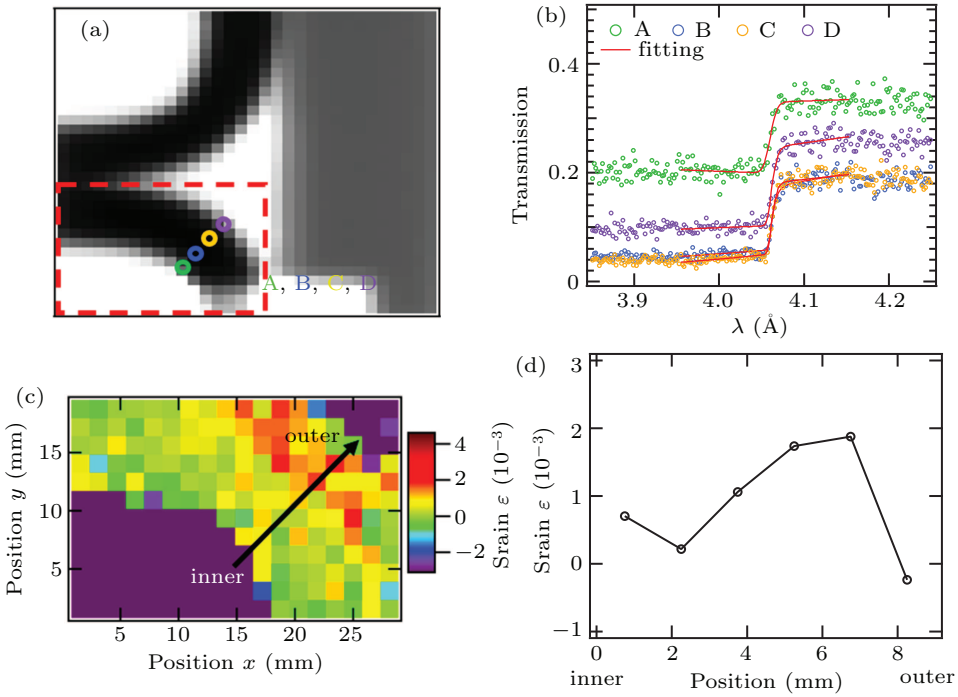


Fig. 5. (a) The ROI of the bent Q235 ferrite steel sample. (b) The fitting results of the selected four points. (c) The residual strain mapping of the ROI. (d) Strain–position curve along the black solid arrow in (c).

In summary, the 2D TOF neutron Bragg-edge imaging has been achieved for the first time in China. The results demonstrate the potential and efficiency of this quantitative technique to visualize the spatial distributions of crystallographic information. As a dedicated neutron imaging instrument at CSNS, ERNI chooses a coupled hydrogen moderator as its neutron source. It has higher flux in the cold neutron range which could covering most Bragg edges of metals. A 35-m flight path could provide a reasonable spectral resolution better than 0.5%. Research and development activities of Bragg-edge imaging are still continued for the ERNI project to serve domestic users of multidisciplinary fields. It can be a key analysis tool of this neutron imaging instrument for materials science and engineering.

References

[1] Li X Y, Zhang Z G, He L H, Avdeev M, Ren Y, Zhao H Z and Wang F W 2020 *Chin. Phys. B* **29** 106101
[2] Wang F W, Zhang P L, Shen B G and Yan Q W 2004 *Chin. Phys.* **13** 918
[3] Wei Y, Ma X Y, Feng Z L, Adroja D, Hillier A, Biswas P, Senyshyn A, Hoser A, Mei J W, Meng Z Y, Luo H Q, Shi Y G and Li S L 2020 *Chin. Phys. Lett.* **37** 107503
[4] Sato H 2018 *J. Imaging.* **4** 7
[5] Kardjilov N, Bacechler S, Bastürk M, Jolie J, Lehmann E, Materna T, Schillinger B and Vontobel P 2003 *Nuclear Instruments and Methods in Physics Research A.* **501** 536
[6] Santisteban J R, Edwards L, Steuwer A and Withers P J 2001 *J. Appl. Cryst.* **34** 289
[7] Kabra S, Kelleher J, Kockelmann W, Gutmann M and Tremsin A 2016 *J. Phys.: Conf. Ser.* **746** 012056
[8] Woracek R, Penumadu D, Kardjilov N, Hilger A, Boin M, Banhart J and Manke I 2014 *Adv. Mater.* **26** 4069
[9] Ziesche R F, Tremsin A S, Huang C, Tan C, Grant P S, Storm M, Brett D J L, Shearing R P and Kockelmann W 2020 *J. Imaging.* **6** 136
[10] Watanabe K, Minniti T, Sato H, Tremsin A S, Kockelmann W, Dalgliesh R and Kiyanagi Y 2019 *Nuclear Inst. Methods in Physics Research A* **944** 162532
[11] Carminati C, Strobl M, Minniti T, Boillat P, Hovind J, Morgano M, Rod T H, Polatidis E, Valsecchi J, Mannes D, Kockelmann W and Kaestner A 2020 *J. Appl. Cryst.* **53** 188
[12] Tremsin A S, Vallerga J V, McPhate J B, Siegmund O H W and Raffanti R 2013 *IEEE Transactions on Nuclear Science.* **60** 578
[13] Shinohara T, Kai T, Oikawa K, Nakatani T, Segawa M, Hiroi K, Su Y H, Ooi M, Harada M, Iikura H, Hayashida H, Parker J D, Matsumoto Y, Kamiyama T, Sato H and Kiyanagi Y 2020 *Rev. Sci. Instrum.* **91** 043302
[14] Minniti T, Watanabe K, Burca G, Pooley D E and Kockelmann W 2018 *Nuclear Inst. Methods in Physics Research A* **888** 184
[15] Chen H S, Wang X L 2016 *Nat. Mater.* **15** 689
[16] Strobl M 2015 *Physics Procedia.* **69** 18
[17] Chen J, Kang L, Lu H L, Luo P, Wang F W and He L H 2018 *Physica B* **551** 370
[18] He L H, Chen J, Lu H L, Luo P, Wu Y D, Kang L, Zhang J C, Zhang J R, Du R, Jia X J, Liang T J and Wang F W 2018 *Neutron News.* **29** 7
[19] Wang S X, Chen J, Tan Z J, Deng S H, Wu Y D, Lu H L, Li S D, Chen W C and He L H 2020 *Chin. Phys. B*
[20] Zhou J R, Zhou X J, Zhou J J, Teng H Y, Yang J Q, Ma Y C, Zhou K, Xia Y G, Xiu Q L, Yang T, Jiang X F, Zhu L, Yang W Q, Yang G A, Xie Y G, Hu B T, Sun Z J and Chen Y B 2020 *Nuclear Inst. Methods in Physics Research A* **962** 163593
[21] Boin M J 2012 *Appl. Cryst.* **45** 603
[22] Pintschovius L, Jung V, Macherauch E and Vöhringer O 1983 *Materials Science and Engineering* **61** 43
[23] van Beeck J, Kouznetsova V G and van Maris M P F HL 2011 *Materials Science and Engineering A* **528** 7207
[24] Lee Y S, Lim J S, Kwon Y N and Moon Y H 2011 *Procedia Engineering* **10** 3333